An engineered biosensor enables dynamic aspartate measurements in living cells

Kristian Davidsen[1,2,†], **Jonathan S Marvin**[3,†*], **Abhi Aggarwal**[3], **Timothy A Brown**[3], **Lucas B Sullivan**[1*]

***For correspondence:**
marvinj@janelia.hhmi.org (JSM);
sullivan@fredhutch.org (LBS)

[†]These authors contributed equally to this work

[1]Human Biology Division, Fred Hutchinson Cancer Center, Seattle, WA, USA; [2]Molecular and cellular biology program, University of Washington, Seattle, WA, USA; [3]Howard Hughes Medical Institute (HHMI), Janelia Research Campus, Ashburn, VA, USA

Abstract Intracellular levels of the amino acid aspartate are responsive to changes in metabolism in mammalian cells and can correspondingly alter cell function, highlighting the need for robust tools to measure aspartate abundance. However, comprehensive understanding of aspartate metabolism has been limited by the throughput, cost, and static nature of the mass spectrometry based measurements that are typically employed to measure aspartate levels. To address these issues, we have developed a GFP-based sensor of aspartate (jAspSnFR3), where the fluorescence intensity corresponds to aspartate concentration. As a purified protein, the sensor has a 20-fold increase in fluorescence upon aspartate saturation, with dose dependent fluorescence changes covering a physiologically relevant aspartate concentration range and no significant off target binding. Expressed in mammalian cell lines, sensor intensity correlated with aspartate levels measured by mass spectrometry and could resolve temporal changes in intracellular aspartate from genetic, pharmacological, and nutritional manipulations. These data demonstrate the utility of jAspSnFR3 and highlight the opportunities it provides for temporally resolved and high throughput applications of variables that affect aspartate levels.

Introduction

The primary tool used by metabolism researchers, mass spectrometry (MS) coupled with either gas chromatography (GCMS) or liquid chromatography (LCMS), involves extracting pools of thousands of cells and measuring the liberated metabolites. This approach is powerful but has significant drawbacks; it requires highly specialized equipment, it is expensive, and sample preparation by chemical extractions homogenizes metabolic differences that may occur amongst different cells in complex samples or across subcellular compartments. Metabolite extraction also consumes precious samples that might otherwise be desirable to analyze over time or with additional outputs. Development of genetically encoded protein sensors (biosensors) over the past two decades has provided new opportunities to visualize the release, production, and depletion of important signaling molecules and metabolites with subsecond and subcellular resolution (reviewed in ***Kostyuk et al.*** (***2019***); ***Koveal et al.*** (***2020***)). Thus, with the trade-off of only monitoring one metabolite per sensor, biosensors provide a solution to many of the problems inherent to metabolite extraction and MS.

Aspartate is amongst the most concentrated metabolites in cells (***Park et al., 2016***), yet it is one of only two amino acids that is not predominantly acquired from the environment. While the

other, glutamate, is made from glutamine by the enzyme glutaminase, no analogous enzyme exists in humans to convert asparagine to aspartate (***Sullivan et al., 2018***). Instead, aspartate must be synthesized by transamination of the tricarboxylic acid (TCA) cycle metabolite oxaloacetate by the cytosolic enzyme GOT1 or the mitochondrial enzyme GOT2. Notably, aspartate synthesis can occur from multiple metabolic sources *via* complex metabolic reactions occurring in both the cytosol and mitochondria, rendering aspartate levels at the whole cell and subcellular levels dependent on multiple metabolic variables. For example, impairments to mitochondrial respiration can deplete aspartate levels and aspartate restoration can reestablish proliferation in cells with defective mitochondria (***Sullivan et al., 2015***; ***Birsoy et al., 2015***; ***Cardaci et al., 2015***; ***Hart et al., 2023***). Alterations to aspartate levels are associated with modifications to cell function in multiple biological processes, including stem cells (***Tournaire et al., 2022***; ***Arnold et al., 2022***), immune cells (***Bailis et al., 2019***), endothelial cells (***Diebold et al., 2019***), and cancer (***Helenius et al., 2021***). In addition, genetic methods to elevate intracellular aspartate can impact biology *in vivo*, increasing tumor growth (***Sullivan et al., 2018***; ***Garcia-Bermudez et al., 2018***) and improving hematopoietic function (***Qi et al., 2021***). Therefore, our understanding of metabolism in multiple biological systems could be improved with the availability of an aspartate biosensor.

We have previously developed a biosensor for glutamate (iGluSnFR) using the *E.coli* glutamate/aspartate binding domain (GltI) linked to circularly permutated GFP (***Marvin et al., 2013***), and subsequently optimized it by modulating its affinity, kinetics, color, and total fluorescence change (SF-iGluSnFR and iGluSnFR3) (***Marvin et al., 2018***; ***Aggarwal et al., 2023***). Since the GltI domain also binds aspartate, albeit at lower affinity than glutamate (***Hu et al., 2008***), we reasoned that subtle modifications to the ligand binding site could switch the relative aspartate/glutamate specificity. We achieved this using a small mutagenesis screen on a precursor to iGluSnFR3 (Supplementary file 1), guided by the crystal structure of glutamate-bound GltI. The resulting biosensor, jAspSnFR3, was characterized *in vitro* and in cells with matched LCMS determined aspartate levels, showing that it accurately reports genetic, pharmacological, and nutritional manipulation of intracellular aspartate.

Results

Protein engineering

We observed that the glutamate sensor, iGluSnFR, binds both glutamate and aspartate, with higher affinity for the former (***Marvin et al., 2013***). To shift the relative affinities of the two ligands, we evaluated the structure of the binding pocket (***Hu et al., 2008***), and sampled all possible amino acid substitutions of residue S72, which interacts with the side-chain carboxylate of bound glutamate (***Figure 1***, panel A). By expressing mutant sensors in bacteria and measuring the fluorescence of bacterial lysate in response to aspartate and glutamate, we identified S72A and S72P as having switched specificity from glutamate to aspartate. S72T, identified in a faster version of iGluSnFR (***Helassa et al., 2018***), also preferentially binds aspartate over glutamate.

As an improved glutamate sensor (iGluSnFR3) was being developed (***Aggarwal et al., 2023***), we took a variant from that process and queried the effect of S72A, S72T, and S72P on aspartate/glutamate affinity. In bacterial cell lysate, S72P maintained the expected shift to a preference for aspartate when inserted into a iGluSnFR3 precursor, and had a higher fluorescence fold increase (F/F) than either S72A or S72T (***Figure 1—figure Supplement 1***, panel A). To further increase specificity of the S72P mutant, we sampled mutations at S27, which also interacts with the carboxylate of bound glutamate. One of those, S27A, had lower affinity for glutamate while mostly maintaining affinity for aspartate (***Figure 1—figure Supplement 1***, panel A). We then moved forward with this variant, and since it is built from a precursor of iGluSnFR3, named it Janelia-developed Aspartate-Sensing Fluorescent Reporter (jAspSnFR3). Since we expected to be using this sensor in cell culture studies, and potentially *in vivo*, over the course of hours or even days, we added a C-terminal red fluorescence protein, mRuby3, to enable correction for expression and movement artefacts. All biochemical characterization is reported with jAspSnFR3-mRuby3. For jAspSnFR3 sig-

nal normalization in cells we used a mix of jAspSnFR3-mRuby3 and nuclear localized RFP.

Further characterization of the sensor found it is yellow-shifted in excitation and emission compared to typical GFP-based sensors, since its chromophore is formed by the triad of GYG and has the T203Y pi-stacking mutations of the Venus yellow fluorescent protein. This yellow-shift facilitates observation deeper into tissues using 2-photon microscopy, as the sensor has high signal fold change and significant 2-photon cross-section at 1040 nm (***Figure 1—figure Supplement 1***, panel B). It has a K_D for aspartate of about 50 µM and binds glutamate and asparagine with K_D greater than 5 mM (***Figure 1***, panel B). It also does not appreciably change its green fluorescence in response to other amino acids (***Figure 1—figure Supplement 2***, panel A). Surprisingly, the mRuby3 component responds to some amino acids at high millimolar concentrations, indicating a non-specific effect, potentially interactions with the C-terminal histidine tag (***Figure 1—figure Supplement 2***, panel B). Notably, this increase in fluorescence is still an order of magnitude lower than the green fluorescence response and it occurs at amino acid concentrations that are unlikely to be achieved in most cell types. The sensor also does not respond to other decoys considered relevant to aspartate metabolism nor to relevant pharmacological treatments (***Figure 1—figure Supplement 2***, panel C). A recently described and concurrently developed biosensor for aspartate is reported to be adversely affected by temperatures higher than 30C, causing lower maximum F/F (***Hellweg et al., 2023***). Our aspartate sensor appears unaffected by temperature up to 37°C, with the same maximum F/F at 37°C as compared to 30C (***Figure 1—figure Supplement 2***, panel D). Like all cpGFP-based sensors, it is sensitive to pH but changes in fluorescence due to aspartate far exceed what one might expect from changes in fluorescence due to physiologically attainable changes in intracellular pH (***Figure 1—figure Supplement 2***, panel E). To determine whether it had the potential to serve as an aspartate biosensor in mammalian cells, we expressed jAspSnFR3 in H1299 cells along with nuclear-RFP. Expression of jAspSnFR3 had no obvious toxic effects and H1299 jAspSnFR3 cells had visible fluorescence in the green channel (***Figure 1***, panel C). As it is the primary substrate for aspartate production, glutamine removal is expected to deplete aspartate levels. Indeed, we found that 24 hours of glutamine withdrawal abolished GFP signal while leaving RFP unchanged. These findings therefore supported the further testing of jAspSnFR3 as a method to quantify aspartate levels over time in live mammalian cells.

jAspSnFR3 reveals the temporal dynamics of aspartate limitation

Having shown that jAspSnFR3-mRuby3 protein can measure the concentration of aspartate *in vitro*, we wanted to test the usefulness of the sensor in cells. To that end, we generated stable cell lines with constitutive expression of jAspSnFR3-mRuby3 or jAspSnFR3 and nuclear localized RFP, and generated single cell clones from each to yield cell lines with uniform expression. In each case, we then normalized GFP sensor signal to RFP signal to control for expression differences within and across cell lines. We also noted that normalization with nuclear RFP and RFP fusion were highly correlated, enabling jAspSnFR3 sensor applications where nuclear RFP labeling is desirable e.g. for counting cells at multiple timepoints using live cell imaging (***Figure 2—figure Supplement 1***, panel C). An important motivation for using a biosensor for tracking aspartate changes is to enable temporal measurements on the same subset of live cells, therefore we used an Incucyte S3 which performs live cell imaging under native cell line growth conditions.

Cellular aspartate levels depend on the availability of metabolic precursors and the activity of several metabolic processes. One such process is the generation of a sufficiently large intracellular NAD+/NADH ratio to drive aspartate precursor synthesis, a process normally maintained through mitochondrial respiration or, in its absence, by treatment with exogenous electron acceptors like pyruvate (***Figure 2***, panel A). Genetic alterations and pharmacological treatments that disrupt mitochondrial respiration can decrease NAD+/NADH and aspartate levels, both of which can be partially restored by supplementation with pyruvate (***Sullivan et al., 2015***; ***Birsoy et al., 2015***). We thus tested the ability of jAspSnFR3 to quantify depletion of intracellular aspartate abundance upon treatment with the mitochondrial complex I inhibitor rotenone and the partial rescue

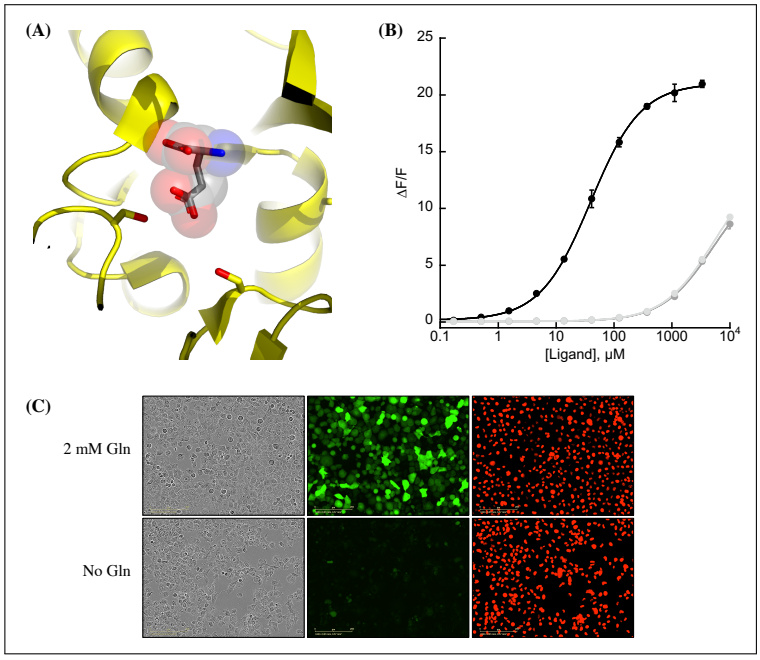

Figure 1. Protein engineering and *in vitro* characterization. (A) Structure of the binding pocket of glutamate-bound GltI (2VHA.pdb) with residues S72 (left) and S27 (right) shown as sticks and bound glutamate as sticks inside transparent spheres. (B) Fluorescence response of purified jAspSnFR3-mRuby3 when titrated with aspartate (black) or glutamate or asparagine (grey tones). Ex. 485 nm (20 nm bandpass), Em. 535 nm (20 nm bandpass). Error bars are s.d. of three technical replicates. (C) Live cell imaging in the phase contrast, GFP and RFP channels of H1299 Nuclear-RFP cells expressing jAspSnFR3 after 24 hours with/without glutamine.

Figure 1—figure supplement 1. Aspartate specificity and excitation/emission spectra.

Figure 1—figure supplement 2. Decoy, temperature and pH sensitivity.

of aspartate by supplementing cells with pyruvate. Titrating rotenone in H1299 cells, we observed a dose dependent decrease in sensor fluorescence with increased rotenone, corresponding to the expected decrease in aspartate synthesis capacity, and a partial restoration of fluorescence in cells co-treated with pyruvate (***Figure 2***, panel B). This observation was extended to different cell lines with different rotenone sensitivities, corroborating the observation of decreased sensor fluorescence upon rotenone treatment and rescue by pyruvate supplementation (***Figure 2—figure Supplement 1***, panel A, B and D).

We next evaluated the ability of the sensor to measure changes in aspartate without requiring treatment with a mitochondrial inhibitor. To this aim, we used CRISPR/Cas9 to generate an H1299 cell line with a double knockout (DKO) of the genes glutamic oxalacetic transaminases 1 and 2 (GOT1/2 DKO), which renders cells unable to synthesize aspartate and therefore dependent on aspartate uptake from the media (***Garcia-Bermudez et al., 2022***). Using these H1299 GOT1/2 DKO cells, we titrated media aspartate and observed that sensor fluorescence decreased upon aspartate withdrawal, approaching a steady-state after approximately 11 hours that corresponded to the aspartate availability in the media (***Figure 2***, panel C). We note that 10 mM media aspartate, a higher concentration than any other amino acid in media, is still unable to rescue sensor signal significantly above aspartate depleted media, confirming previous observations that aspartate has poor cell permeability and often requires 20 mM aspartate or more to robustly contribute to intracellular aspartate pools (***Sullivan et al., 2018***).

Metformin has slower inhibitor kinetics compared to rotenone

Metformin is a commonly used diabetes treatment that has been shown to act as a mitochondrial complex I inhibitor (***Owen et al., 2000***; ***El-Mir et al., 2000***; ***Andrzejewski et al., 2014***; ***Wheaton***

et al., 2014) and can decrease intracellular aspartate levels in a dose responsive way (*Gui et al., 2016*). Whereas rotenone is a lipophilic molecule that can cross the cell membrane and act rapidly, metformin is hydrophilic and poorly permeable to most cells, resulting in comparatively delayed kinetics for metformin to decrease mitochondrial respiration in intact cells. As rotenone and metformin are often used interchangeably as complex I inhibitors, we wondered whether they have an equivalent temporal effect on aspartate or if the delayed effects of metformin on mitochondrial inhibition would similarly delay its effects on aspartate levels. To test this, we treated cells with two doses each of rotenone and metformin with roughly equivalent aspartate lowering effects and followed the sensor signal over time (*Figure 2*, panel E). We observed that the aspartate depleting effects of metformin acted slower than rotenone, with 30 nM rotenone reaching steady-state after 20h and 2 mM metformin reaching a similar sensor response after almost 40h. These data therefore provide orthogonal confirmation of the differential kinetics of these drugs on cell metabolism and highlight the temporal opportunities enabled by measuring aspartate levels by jAspSnFR3.

Asparagine salvage diverts glutamine consumption

In most cancer cell lines, intracellular aspartate is derived primarily from glutamine oxidation, thus making glutamine depletion an entry point for affecting aspartate metabolism. It has previously been reported that asparagine, a product of aspartate metabolism, becomes essential upon glutamine starvation (*Pavlova et al., 2018*; *Zhang et al., 2014*). We hypothesize that asparagine becomes essential in these conditions because glutamine starvation decreases synthesis of aspartate, slowing asparagine production, and because asparagine supplementation spares aspartate consumption, allowing it to be redirected into other essential fates. However, it has been difficult to measure metabolic changes during glutamine limitation because continuous glutamine consumption during the course of the experiment will result in progressive glutamine depletion and further developing metabolic effects. One solution to this problem is to measure the temporal changes in aspartate levels over the course of glutamine starvation, a possibility enabled by fluorescence based measurements of aspartate using jAspSnFR3. Indeed, we found that full glutamine depletion has a rapid and drastic effect on sensor signal and that this effect was delayed by adding back glutamine (*Figure 2*, panel F). Aspartate signal did not robustly correlate with the concentration of glutamine in the media in the short term, but instead we found that higher amounts of glutamine in the media delayed the time until aspartate depletion, presumably corresponding to the time at which glutamine is fully depleted and unable to support further aspartate synthesis. Furthermore, we found that adding 1 mM asparagine delayed the decrease in sensor signal, suggesting that when asparagine can be salvaged from the media it diverts glutamine consumption that would otherwise be purposed for asparagine synthesis via aspartate consumption. We note that, as this data is produced in real-time, the method can be used to dynamically find the optimal sampling times to measure and compare intracellular levels of all the metabolites relevant to glutamine starvation using mass spectrometry.

jAspSnFR3 signal correlates with intracellular aspartate concentration

It is an important requirement for an aspartate sensor that it reflects the intracellular concentration of aspartate over a biologically relevant range for several cell lines. Reference points for the intracellular aspartate concentration can be generated using metabolite extraction and LCMS, but it is important to note that this technique reports the total amount of aspartate summed across all compartments, which can differ in their aspartate concentration (*Chen et al., 2016*). The LCMS derived concentration also does not reflect protein crowding, aspartate binding to enzymes, or other factors that would affect the free aspartate concentration. Nevertheless, LCMS is the standard approach in studying metabolism and has previously been used to correlate aspartate levels with cell proliferation (*Gui et al., 2016*; *Hart et al., 2023*). Thus, we titrated mitochondrial inhibitors of complex I (rotenone and metformin) and complex III (antimycin A), with or without pyruvate rescue, in three different cell lines and waited 24 hours until aspartate had reached near steady-state levels

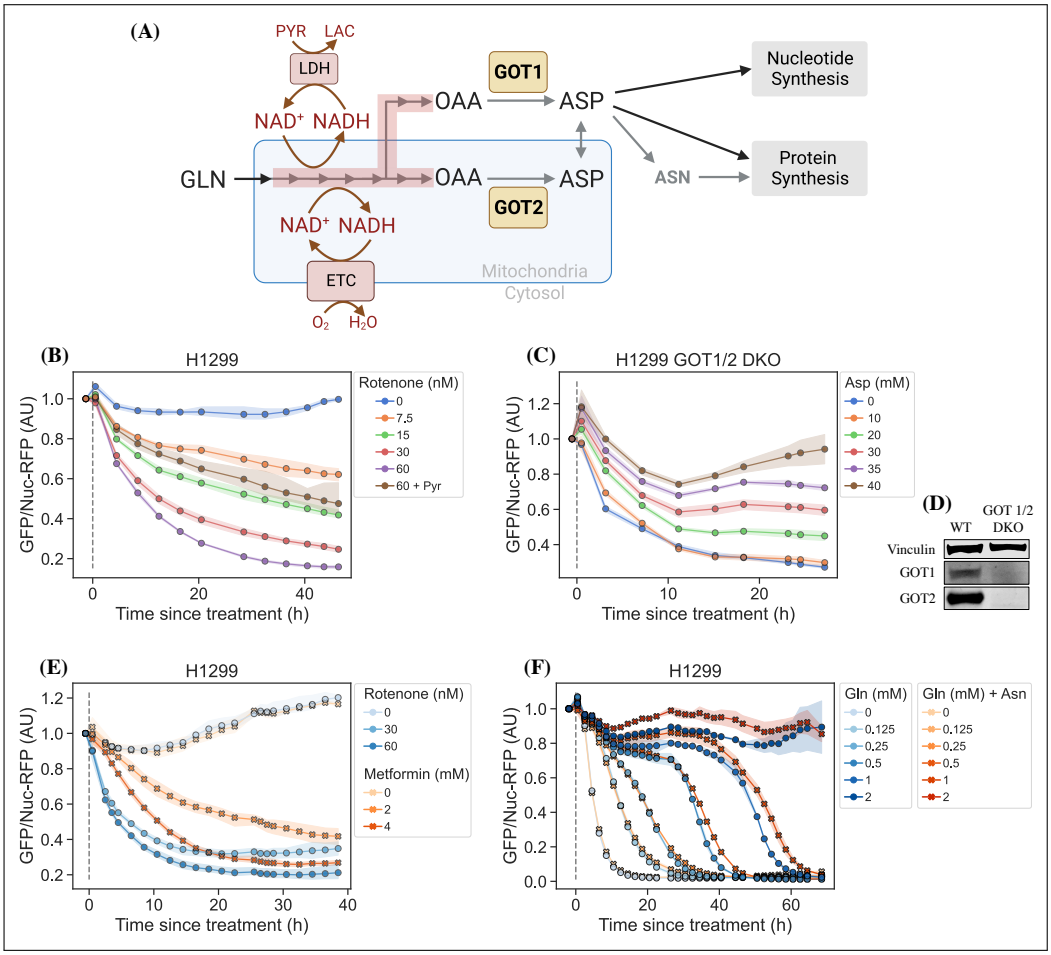

Figure 2. jAspSnFR3 resolves temporal aspartate changes in live cells. (A) Overview of aspartate metabolism and the effect of glutamine depletion, mitochondrial inhibition, GOT1/2 knockout and pyruvate/asparagine supplementation. GLN, glutamine. ETC, electron transport chain. LDH, lactate dehydrogenase. OAA, oxaloacetic acid. ASP, aspartate. ASN, asparagine. For (B), (C), (E) and (F), sensor signal over time shown as RFP normalized jAspSnFR3 signal following various perturbations of live cells. All experiments shown are normalized to a pre-treatment scan, then treated with the specified drug or amino acid and scanned 30 min following treatment. Grey dashed lines indicate the time of treatment. (B) H1299 cells treated with a rotenone titration and rescued by co-treatment with pyruvate. (C) H1299 GOT1/2 double knockout cells grown in media with 40 mM aspartate, washed thrice in media without aspartate and then changed into media with a titration of aspartate. (D) Western blot verification of H1299 GOT1/2 double knockout. (E) H1299 cells treated with either rotenone or metformin to compare inhibitor kinetics. (F) H1299 cells changed into media with a titration of glutamine with or without 1 mM asparagine. Markers indicate the average using available well replicates and are superimposed on a bootstrapped 95% confidence interval colored using the same color code as the markers. AU, arbitrary unit.

Figure 2—figure supplement 1. Rotenone titration in different cell lines.

Figure 2—figure supplement 2. Narrow range glutamine limitation.

before conducting a final measurement of sensor fluorescence, followed by immediate metabolite extraction and quantitative LCMS measurements of aspartate levels using isotope dilution. We then compared sensor signals to LCMS derived aspartate concentrations and fitted a Hill curve to infer the intracellular aspartate concentrations at half-maximum sensor signal (***Figure 3***). For all three cell lines, we observe a monotonically increasing relationship between sensor signal and intracellular aspartate concentration, covering around two orders of magnitude. We also observe no relationship between sensor signal and intracellular glutamate levels (***Figure 3—figure Supplement 1***). These observations validate the utility of our sensor in a biologically relevant range of

aspartate concentrations without interference from glutamate.

Interestingly, the intracellular aspartate concentrations at half-maximum sensor fluorescence is more than 17 fold higher than the aspartate K_D determined by *in vitro* characterization of the sensor. While the numbers inferred for intracellular aspartate are only point estimates, it is highly unlikely that they are inaccurate to this degree. We speculate that the apparent cytosolic aspartate concentration is likely lower than the total aspartate concentration summed across all compartments. This suggests that binding of aspartate by jAspSnFR3 is in competition with other proteins and highlights that another advantage of using a biosensor is that measurements are made relative to their native environment.

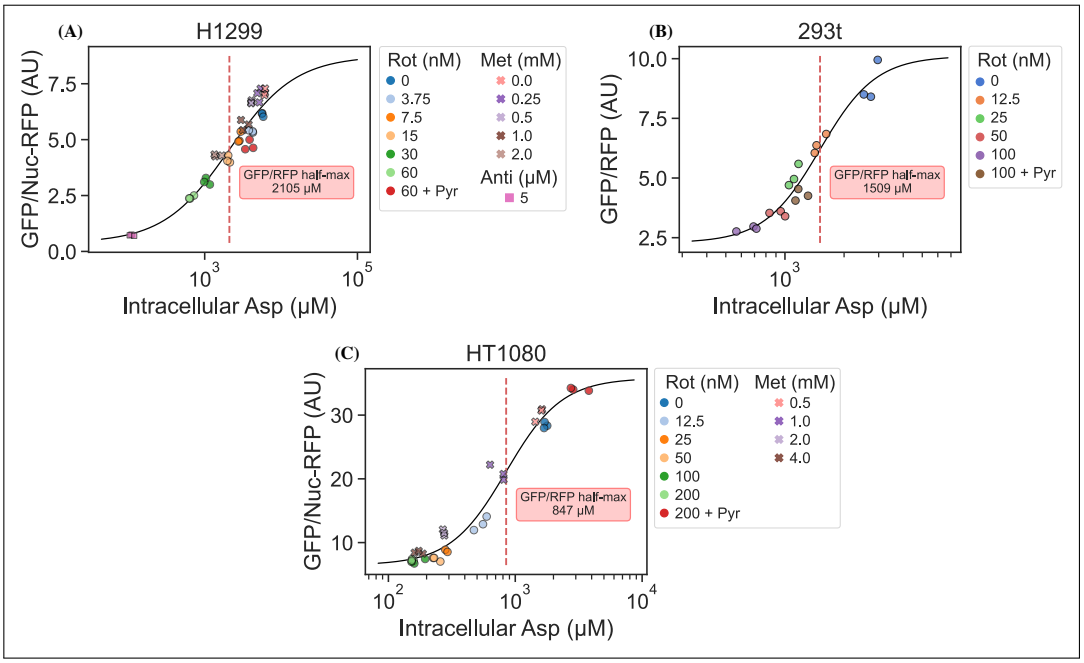

Figure 3. jAspSnFR3 signal predicts LCMS measured intracellular aspartate concentration. A Hill equation with top and bottom asymptotes, midpoint and slope as free variables is fitted to the datapoints and shown by the black line. The intracellular aspartate concentration at the inferred half maximum of RFP normalized jAspSnFR3 signal is reported in the red inserts. (A) Rotenone, metformin and antimycin A titrations in H1299 cells. (B) Rotenone titration in HEK293t cells. (C) Rotenone and metformin titrations in HT1080 cells. Markers indicate a single well from which both LCMS and jAspSnFR3 data was collected. Replicate wells have identical color and marker shape. AU, arbitrary unit.

Figure 3—figure supplement 1. jAspSnFR3 signal does not correlate with glutamate concentration.

Discussion

A biosensor for aspartate is an important step towards improved understanding of aspartate metabolism. We have shown that our jAspSnFR3 sensor can resolve temporal changes in intracellular aspartate to answer questions that would be impractical using LCMS. In most studies involving aspartate metabolism, metabolite extraction is performed 6-16 hours after treatment with the implicit assumption that this is enough time to reach metabolic steady-state. Using our sensor, we have shown that the time to reach steady-state can be much longer and depends on the treatment. Future studies seeking to understand the effects of treatments affecting aspartate levels can therefore use real-time measurements using jAspSnFR3 to determine when cells have reached steady-state and then perform metabolite extraction for LCMS.

Recently, a concurrently developed aspartate sensor based on SF-iGluSnFR was reported by another group (***Hellweg et al., 2023***). That aspartate sensor started with the S72A mutation, but then included 6 additional mutations identified by a combination of targeted screening and deep

mutational scanning. Our design differs from the one by ***Hellweg et al.*** (***2023***) by 25 mutations (Supplementary file 1). Notably, we achieved aspartate selectivity by generating only two mutations in the binding pocket of its precursor, and so the majority of these amino acid differences derive from us building off the next generation precursor for iGluSnFR3, which has increased F/F compared to iGluSnFR. Indeed, the sensor described here appears to have a larger signal change both *in vitro* and in live cells, although head-to-head comparisons have not been performed. Importantly, while the sensor from ***Hellweg et al.*** (***2023***) is adversely affected by temperature at 37°C, our sensor is not affected, allowing us to perform cell culture experiments at standard incubation conditions. Another difference is that our jAspSnFR3 sensor has a higher affinity for all three relevant ligands (aspartate, asparagine, and glutamate); however, we found no discernible effect of treatment with 1 mM asparagine on sensor signal in cell culture experiments and found no correlation between intracellular glutamate concentration and sensor fluorescence across treatment conditions (***Figure 3—figure Supplement 1***). Collectively, we conclude that the jAspSnFR3 aspartate sensor reported here has biochemical features that makes it ideal for measuring intracellular aspartate levels in live cells.

In summary, we report a novel fluorescence based biosensor that enables dynamic measurements of aspartate. This tool is free of significant interference from relevant metabolites in physiological intracellular systems and can resolve changes in aspartate from diverse treatment conditions in live cells over time. This approach to measuring aspartate will also have advantages compared to LCMS based metabolomics, including enabling high throughput experiments to identify variables that affect aspartate levels, such as testing the effects of a drug library on cells in multiwell plates or using FACS based selection during genetic screens. Another potential use for this sensor would be to dissect compartmentalized metabolism, with mitochondria being a critical target. Altogether, adoption of jAspSnFR3 to measure aspartate levels will therefore provide novel opportunities to understand this critical node of cell metabolism.

Methods and Materials

Sensor engineering and screening

The starting template for jAspSnFR3 was a variant along the path of making iGluSnFR3 (sequence information in Supplementary file 1). Site saturation mutagenesis at positions S72 and S27 was achieved by the uracil template method (***Kunkel, 1985***). Mutant libraries (maximum theoretical diversity of 20 each) were transformed into T7 express cells. Individual colonies were picked into a 96-well plate containing auto-induction media (***Studier, 2005***) and shaken at 30C for 18-24 hours, then harvested by centrifugation. Cell pellets were resuspended in PBS and repelleted by centrifugation 5 times over, then frozen as pellets overnight. The frozen 96-well plate was thawed by addition of room temperature PBS, agitated by vortexing to resuspend and lyse cells, and then pelleted again. 100 µL clarified lysate was added to each of two black 96-well plates and its fluorescence was measured. Aspartate or glutamate was added (final concentration 100 µM) and fluorescence was measured again. Wells that had a higher F/F for aspartate than glutamate were isolated, titrated with aspartate and glutamate, and sequenced. After confirming that S72P was the most selective variant for aspartate from a library of S72X, a library of S27X was made in the background of S72P. The selection process was repeated, and S72P+S27A was identified as the "best" aspartate sensor and named jAspSnFR3. mRuby3 was subsequently cloned at the C-terminus and this construct was named jAspSnFR3-mRuby3.

Protein expression and purification

For large scale protein expression and purification, jAspSnFR3-mRuby3 was transformed into T7 express cells and a single colony was grown in 300 mL auto-induction media (***Studier, 2005***) at 30C for 18 hours. Cells were pelleted by centrifugation at 6000g, resuspended in PBS and 1 M NaCl and frozen. The resuspended cell pellet was thawed, sonicated on ice (5 sec on, 5 sec off,

10 min), and centrifuged at 6000g to remove cellular debris. The lysate was further clarified by centrifugation at 350,000g for 1 hour, and then purified by IMAC on a HisTrap FF column, with a 2 mL/min flow rate and elution from 0 to 200 mM imidazole over 120 mL. Fluorescent fractions were pooled, concentrated by ultrafiltration, and dialyzed in PBS to remove endogenously bound ligands. Protein concentration was determined by alkaline denaturation, and measurement at A447 (Ext. Coeff. 44,000 M-1 cm-1).

Sensor biochemical characterization

In vitro fluorescence measurements were performed on a Tecan Spark plate reading fluorimeter at 28C, with the exception of the controlled temperature measurement, in which a BioTek Cytation 5 was used. Concentrated jAspSnFR3-mRuby3 protein was diluted to 0.2 µM in PBS for all measurements. Decoy amino acids and pharmacologues were purchased from Sigma-Aldrich and solvated as 100 mM stocks in PBS, with the exception of rotenone, which was resuspended in DMSO. Titrations were performed by making serial dilutions (1:2) of the stock compound into PBS, and adding 10 µL of that to 100 µL of 0.2 µM protein solution. Fluorescence was measured before addition of compound, and F/F was calculated as (F(treatment)-F(initial))/F(initial).

Two-photon cross sections were collected for 1 µM solutions of protein in PBS with or without 10 mM aspartate, excited by pulses from a mode-locked Ti:Sapphire laser (Chameleon Ultra, Coherent, 80 MHz, 140-fs pulse width, 1 mW power at the focus). Emission was detected by an avalanche photodiode (PDM Series, Micro Photon Devices) with a 550 nm filter (88-nm bandpass).

Cell culture

Cell lines were acquired from ATCC (HEK293T, H1299, HT1080) and tested to be free from mycoplasma (MycoProbe, R&D Systems). Cells were maintained in Dulbecco's Modified Eagle's Medium (DMEM) (Gibco, 50-003-PB) supplemented with 3.7 g/L sodium bicarbonate (Sigma-Aldrich, S6297), 10% fetal bovine serum (FBS) (Gibco, 26140079) and 1% penicillin-streptomycin solution (Sigma-Aldrich, P4333). Cells were incubated in a humidified incubator at 37°C with 5% CO2.

Generation of nuclear RFP cell lines

Nuclear RFP cell lines were generated using 1e5 transducing units of EF1A-nuclear RFP lentivirus (Cellomics Technology, PLV-10205-50) by spinfection. Cells were seeded at 50% confluency in 6 well dishes, lentivirus was added to fresh media with 8 µg/µL polybrene, then added to cells and followed by centrifugation (900g, 90 mins, 30°C). Two days after infection, cells were sorted for high RFP expression using fluorescence-activated cell sorting (FACS). High RFP cells were then expanded and single-cell cloned by limiting dilution, plating 0.5 cells/well on a 96 well plate. Plates were then screened for RFP expression and localization using Incucyte S3 (Sartorius) and a suitable clone chosen, expanded, and used for all subsequent experiments.

Lentiviral production and stable cell line generation

jAspSnFR3 and jAspSnFR3-mRuby3 were first cloned into entry vector pENTR1A (Fisher, A10462) using NEBuilder HiFI DNA Assembly Cloning Kit (New England BioLabs, E2621). These donor constructs were then used to transfer their insert into destination vectors: pLX304-CMV-Blast (Addgene, 25890), pLenti-CMV-Hygro (w117-1) (Addgene, 17454 a gift from Eric Campeau & Paul Kaufman), or pLX304-CAG-Blast using LR Clonase II (Fisher, 11791100). pLX304-CAG-Blast was generated in house by swapping the CMV promoter region of pLX304-CMV-Blast with a CAG promoter provided on synthetic DNA (Integrated DNA Technologies). Each plasmid sequence was verified by whole plasmid sequencing (Plasmidsaurus). Lentivirus was generated by co-transfection of HEK293T cells with destination vector plasmid DNA and the packaging plasmids pMDLg/pRRE (Addgene, 12251), pRSV-Rev, (Addgene, 12253) and pMD2.G (Addgene, 12259) using FuGENE transfection reagent (Fisher, PRE2693) in DMEM (Fisher, MT10017CV) without FBS or penicillin-streptomycin. The supernatant containing lentiviral particles was filtered through a 0.45 µM membrane (Fisher,

9720514) and was supplemented with 8 µg/µL polybrene (Sigma, TR-1003-G) prior to infection. For infection, cells were seeded at 50% confluency in 6 well dishes and centrifuged with lentivirus (900g, 90 mins, 30°C). After 24 hours the media was replaced with fresh media and after 48 hours cells were treated with either 1 µg/mL blasticidin (Fisher, R21001) or 150 µg/mL hygromycin (Sigma-Aldrich, H7772-1G) and maintained in selection media until all uninfected control cells died. After selection, cells were expanded and single-cell cloned by limiting dilution, plating 0.5 cells/well using 2-3 96 well plates. These clones were incubated until 10-30% confluency and screened for high GFP and RFP signal using Incucyte S3 (Sartorius). The highest expressing monoclonal cells were selected and further expanded on 6 well plates and again screened for fluorescence using the Incucyte. From this a single clone was chosen, expanded and used for all subsequent experiments. Different cell lines received different vector-sensor combinations: HEK293T cells were infected with pLX304-CAG-jAspSnFR3-mRuby3 (blasticidin), HT1080 with pLenti-jAspSnFR3-mRuby3 (hygromycin) and HT1080, H1299 and H1299 GOT1/2 DKO cells expressing nuclear RFP were infected with pLenti-jAspSnFR3 (hygromycin).

Generation of GOT1/2 double knockout (DKO) cells

Protocol and guide RNA generation was identical to that described in ***Hart et al.*** (***2023***). Briefly, three chemically synthesized 2'-O-methyl 3'phosphorothioate-modified single guide RNA (sgRNA) sequences targeting GOT1 and GOT2 were purchased (Synthego; ***Table 1***). A pool of all six sgRNAs for GOT1 and GOT2 were resuspended in nuclease-free water, combined with SF buffer (Lonza, V4XC-2032), and sNLS-spCas9 (Aldevron, 9212). 200,000 H1299 cells were resuspended in the resulting solution containing ribonucleoprotein complexes (RNPs) and electroporated using a 4D-Nucleofector (Amaxa, Lonza). Nucleofected cells were then expanded and single-cell cloned by limiting dilution by plating 0.5 cells/well in a 96 well plate. Gene knockout was confirmed using western blots.

Table 1. CRISPR guides.

Gene	sgRNA sequence (5'-3')
GOT1	CAGUCAUCCGUGCGAUAUGC
	GCACGGAUGACUGCCAUCCC
	CGAUCUUCUCCAUCUGGGAA
GOT2	UUUCUCAUUUCAGCUCCUGG
	CGGACGCUAGGCAGAACGUA
	UCCUUCCACUGUUCCGGACG

Intracellular jAspSnFR3 measurements

Experiments were conducted in DMEM without pyruvate (Corning 50-013-PB) supplemented with 3.7 g/L sodium bicarbonate 10% dialyzed fetal bovine serum (FBS) (Sigma-Aldrich, F0392) and 1% penicillin-streptomycin solution. To start an experiment, cells were trypsinized (Corning, 25051CI), resuspended in media, counted using a coulter counter (Beckman Coulter, Multisizer 4) and seeded onto 24-well dishes (Nunc, 142475) with an initial seeding density of 50,000, 70,000, 70,000 or 150,000 cells/well for H1299, H1299 GOT1/2 DKO, HT1080 and HEK293T, respectively. After 24h (H1299, HT1080, HEK293T) or 48h (H1299 GOT1/2 DKO) incubation, treatment was added and plates moved into an Incucyte S3 (Sartorius) live cell imaging platform inside a humidified incubator at 37°C with 5% CO2. Rotenone (Sigma-Aldrich, R8875), metformin (Sigma-Aldrich, D150959) and antimycin A (Sigma-Aldrich, A8674) treatments were spiked-in as 20x solutions in water and the 2 mM pyruvate (Sigma-Aldrich, P8574) was added as 500x stock in water. For treatments with varying media aspartate (Sigma-Aldrich, A7219) or glutamine (Sigma-Aldrich, G5792), wells were thrice washed and filled with media deplete of the given amino acid, then it was added as a spike-in at the specified concentration from a 20x solutions in water. For plates receiving asparagine

(Sigma-Aldrich, A7094), this was added to 1 mM from a 20x solution in water, with vehicle wells receiving water. Live cell imaging was performed on the Incucyte S3 using the GFP and RFP channels with default exposure times. Images were processed using the associated Incucyte software to subtract background, define areas of cell confluence and GFP/RFP signal and extract the sum of the fluorescence signal in these areas. The data for the GFP signal, RFP signal, GFP/RFP ratio and confluence for each well at each timepoint was exported and used for further data processing using Python code. The jAspSnFR3 signal (GFP channel) was normalized to an RFP signal, either as a stably expressed nuclear localized RFP (Nuc-RFP) or mRuby3 C-term fusion to jAspSnFR3. For temporal measurements the first scan was made 30 min after treatment with subsequent scans indicated on relevant plots. For some experiments a pre-treatment scan was made shortly prior to treatment to normalize the data to this point. For comparisons of near steady-state measurements of GFP/RFP versus mass spectrometry based metabolite measurements, a single scan was made 24h after treatment, the plate was then quickly moved to ice and metabolite extraction performed (see below). Another plate was processed in parallel for cell volume determination using a coulter counter and averaging across three replicate wells. The normalized jAspSnFR3 signal as a function of intracellular aspartate concentration, $f(c)$, was fitted by a baseline shifted Hill curve:

$$f(c) = t + \frac{b - t}{1 + (c/m)^s}$$

With t, b being the top and bottom of the curve, respectively, describing the upper and lower asymptotes of normalized jAspSnFR3 signal. The curve slope is described by s, also known as Hill coefficient, and the midpoint (m) describes the intracellular aspartate concentration at half maximum jAspSnFR3 signal. The curve parameters were fitted to the data using the Broyden–Fletcher–Goldfarb–Shann (BFGS) algorithm with an upper bound constraint on the top of the curve of 1.2 times the maximum observed normalized jAspSnFR3 signal in any of the conditions on the same plot. Note that this curve is not intended to represent a mechanistic model of the binding kinetics, rather the purpose is to infer a reasonable estimate of the intracellular aspartate concentration at half maximum jAspSnFR3 signal.

Metabolite extraction

For polar metabolite extraction, a plate was move to ice and the media was thoroughly aspirated. For H1299 and HT1080 cells, wells were washed once with cold saline (Fisher, 23293184). For HEK293T cells, washing was omitted due to weak cell adherence. Then, 1 mL 80% HPLC grade methanol in HPLC grade water was added, cells were scraped with the back of a P1000 pipet tip and transferred to Eppendorf tubes. Tubes were centrifuged (17,000g, 15 mins, 4°C) and 800 µL of the supernatant containing polar metabolites was transferred to a new centrifuge tube and placed in a centrivap until dry.

Intracellular amino acid concentration measurements by isotope dilution

Dried samples were reconstituted with 40 µL 80% HPLC grade methanol containing 5 µM U-13C, U-15N labelled canonical amino acid mix (Cambridge Isotope Laboratories, MSK-CAA-1) and transferred to vials for measurement by LCMS. The peak area for each amino acid was divided by its labelled standard to derive the response ratio. The response ratio was then mapped to a calibration curve to infer the amino acid concentration and finally the intracellular concentration was calculated by correcting for each step introducing a dilution, including the use of the total cell volume. To make the calibration curves a non-labelled amino acid mixture was made from an analytical amino acid standard without glutamine and asparagine (Sigma-Aldrich, A9906-1ML) and added glutamine (Sigma-Aldrich, 76523-100MG) and asparagine (Sigma-Aldrich, 51363-100MG) to match the concentration of the other amino acids. Using this mix, three replicates of a 12 point 2-fold dilution series was made with a max concentration of 500 µM and a volume per dilution of 40 µL. These were placed in a centrivap until dry and reconstituted with 40 µL 80% HPLC grade methanol

containing 5 µM U-13C, U-15N labelled canonical amino acid mix (Cambridge Isotope Laboratories, MSK-CAA-1) and transferred to vials for measurement by LCMS. The peak area for each amino acid was divided by its labelled standard to derive the response ratio, then the best fitting calibration curves for each amino acid were chosen among either linear, power or a second-degree polynomial. Each calibration curve was manually inspected for proper fit and measurements below or above the concentration range of the dilution series were discarded.

Liquid Chromatography-Mass Spectrometry (LCMS)

Metabolite quantitation was performed using a Q Exactive HF-X Hybrid Quadrupole-Orbitrap Mass Spectrometer equipped with an Ion Max API source and H-ESI II probe, coupled to a Vanquish Flex Binary UHPLC system (Thermo Scientific). Mass calibrations were completed at a minimum of every 5 days in both the positive and negative polarity modes using LTQ Velos ESI Calibration Solution (Pierce). Polar Samples were chromatographically separated by injecting a sample volume of 1 L into a SeQuant ZIC-pHILIC Polymeric column (2.1 x 150 mm 5 mM, EMD Millipore). The flow rate was set to 150 mL/min, autosampler temperature set to 10 °C, and column temperature set to 30 °C. Mobile Phase A consisted of 20 mM ammonium carbonate and 0.1 % (v/v) ammonium hydroxide, and Mobile Phase B consisted of 100% acetonitrile. The sample was gradient eluted (%B) from the column as follows: 0-20 min.: linear gradient from 85% to 20% B; 20-24 min.: hold at 20% B; 24-24.5 min.: linear gradient from 20% to 85% B; 24.5 min.-end: hold at 85% B until equilibrated with ten column volumes. Mobile Phase was directed into the ion source with the following parameters: sheath gas = 45, auxiliary gas = 15, sweep gas = 2, spray voltage = 2.9 kV in the negative mode or 3.5 kV in the positive mode, capillary temperature = 300 °C, RF level = 40 %, auxiliary gas heater temperature = 325°C. Mass detection was conducted with a resolution of 240,000 in full scan mode, with an AGC target of 3,000,000 and maximum injection time of 250 msec. Metabolites were detected over a mass range of 70-850 m/z. Quantitation of all metabolites was performed using Tracefinder 4.1 (Thermo Scientific) referencing an in-house metabolite standards library using 5 ppm mass error.

Data analysis and plotting

All data processing, curve fitting, plotting and statistics for experiments involving jAspSnFR3 expressed in cell lines was made using Python code and data available on Github: www.github.com/krdav/Aspartate-sensor

Plasmid availability

Submitted to Addgene under article ID 28238106.

Acknowledgement

We would like to acknowledge Kaspar Podgorski for pre-publication plasmid access to iGluSnFR3 variants and Ronak Patel for the 2P spectral analysis.

Funding

This research was supported by the Proteomics & Metabolomics Shared Resource of the Fred Hutch/University of Washington/Seattle Children's Cancer Consortium (P30 CA015704). L.B.S. acknowledges support from the National Institute of General Medical Sciences (NIGMS; R35GM147118). J.S.M. and T.A.B. are funded by the Howard Hughes Medical Institute.

References

Aggarwal A, Liu R, Chen Y, Ralowicz AJ, Bergerson SJ, Tomaska F, Mohar B, Hanson TL, Hasseman JP, Reep D, Tsegaye G, Yao P, Ji X, Kloos M, Walpita D, Patel R, Mohr MA, Tillberg PW, GENIE Project Team, Looger LL, et al. Glutamate indicators with improved activation kinetics and localization for imaging synaptic transmission. Nat Methods. 2023 May; .

Andrzejewski S, Gravel SP, Pollak M, St-Pierre J. Metformin directly acts on mitochondria to alter cellular bioenergetics. Cancer Metab. 2014 Aug; 2:12.

Arnold PK, Jackson BT, Paras KI, Brunner JS, Hart ML, Newsom OJ, Alibeckoff SP, Endress J, Drill E, Sullivan LB, Finley LWS. A non-canonical tricarboxylic acid cycle underlies cellular identity. Nature. 2022 Mar; p. 1–5.

Bailis W, Shyer JA, Zhao J, Canaveras JCG, Al Khazal FJ, Qu R, Steach HR, Bielecki P, Khan O, Jackson R, Kluger Y, Maher LJ 3rd, Rabinowitz J, Craft J, Flavell RA. Distinct modes of mitochondrial metabolism uncouple T cell differentiation and function. Nature. 2019 Jul; 571(7765):403–407.

Birsoy K, Wang T, Chen WW, Freinkman E, Abu-Remaileh M, Sabatini DM. An Essential Role of the Mitochondrial Electron Transport Chain in Cell Proliferation Is to Enable Aspartate Synthesis. Cell. 2015 Jul; 162(3):540–551.

Cardaci S, Zheng L, MacKay G, van den Broek NJF, MacKenzie ED, Nixon C, Stevenson D, Tumanov S, Bulusu V, Kamphorst JJ, Vazquez A, Fleming S, Schiavi F, Kalna G, Blyth K, Strathdee D, Gottlieb E. Pyruvate carboxylation enables growth of SDH-deficient cells by supporting aspartate biosynthesis. Nat Cell Biol. 2015 Oct; 17(10):1317–1326.

Chen WW, Freinkman E, Wang T, Birsoy K, Sabatini DM. Absolute Quantification of Matrix Metabolites Reveals the Dynamics of Mitochondrial Metabolism. Cell. 2016 Aug; 166(5):1324–1337.e11.

Diebold LP, Gil HJ, Gao P, Martinez CA, Weinberg SE, Chandel NS. Mitochondrial complex III is necessary for endothelial cell proliferation during angiogenesis. Nat Metab. 2019 Jan; 1(1):158–171.

El-Mir MY, Nogueira V, Fontaine E, Averet N, Rigoulet M, Leverve X. Dimethylbiguanide Inhibits Cell Respiration via an Indirect Effect Targeted on the Respiratory Chain Complex I *. J Biol Chem. 2000 Jan; 275(1):223–228.

Garcia-Bermudez J, Badgley MA, Prasad S, Baudrier L, Liu Y, La K, Soula M, Williams RT, Yamaguchi N, Hwang RF, Taylor LJ, de Stanchina E, Rostandy B, Alwaseem H, Molina H, Bar-Sagi D, Birsoy K. Adaptive stimulation of macropinocytosis overcomes aspartate limitation in cancer cells under hypoxia. Nat Metab. 2022 Jun; 4(6):724–738.

Garcia-Bermudez J, Baudrier L, La K, Zhu XG, Fidelin J, Sviderskiy VO, Papagiannakopoulos T, Molina H, Snuderl M, Lewis CA, Possemato RL, Birsoy K. Aspartate is a limiting metabolite for cancer cell proliferation under hypoxia and in tumours. Nat Cell Biol. 2018 Jul; 20(7):775–781.

Gui DY, Sullivan LB, Luengo A, Hosios AM, Bush LN, Gitego N, Davidson SM, Freinkman E, Thomas CJ, Vander Heiden MG. Environment Dictates Dependence on Mitochondrial Complex I for NAD+ and Aspartate Production and Determines Cancer Cell Sensitivity to Metformin. Cell Metab. 2016 Nov; 24(5):716–727.

Hart ML, Quon E, Vigil ALBG, Engstrom IA, Newsom OJ, Davidsen K, Hoellerbauer P, Carlisle SM, Sullivan LB. Mitochondrial redox adaptations enable alternative aspartate synthesis in SDH-deficient cells. Elife. 2023 Mar; 12.

Helassa N, Dürst CD, Coates C, Kerruth S, Arif U, Schulze C, Wiegert JS, Geeves M, Oertner TG, Török K. Ultrafast glutamate sensors resolve high-frequency release at Schaffer collateral synapses. Proc Natl Acad Sci U S A. 2018 May; 115(21):5594–5599.

Helenius IT, Madala HR, Yeh JRJ. An Asp to Strike Out Cancer? Therapeutic Possibilities Arising from Aspartate's Emerging Roles in Cell Proliferation and Survival. Biomolecules. 2021 Nov; 11(11).

Hellweg L, Pfeifer M, Chang L, Tarnawski M, Bergner A, Kress J, Hiblot J, Reinhardt J, Johnsson K, Leippe P. Engineering of a biosensor for intracellular aspartate. bioRxiv. 2023; https://www.biorxiv.org/content/early/2023/05/04/2023.05.04.537313, doi: 10.1101/2023.05.04.537313.

Hu Y, Fan CP, Fu G, Zhu D, Jin Q, Wang DC. Crystal structure of a glutamate/aspartate binding protein complexed with a glutamate molecule: structural basis of ligand specificity at atomic resolution. J Mol Biol. 2008 Sep; 382(1):99–111.

Kostyuk AI, Demidovich AD, Kotova DA, Belousov VV, Bilan DS. Circularly Permuted Fluorescent Protein-Based Indicators: History, Principles, and Classification. Int J Mol Sci. 2019 Aug; 20(17).

Koveal D, Díaz-García CM, Yellen G. Fluorescent Biosensors for Neuronal Metabolism and the Challenges of Quantitation. Curr Opin Neurobiol. 2020 Aug; 63:111–121.

Kunkel TA. Rapid and efficient site-specific mutagenesis without phenotypic selection. Proc Natl Acad Sci U S A. 1985 Jan; 82(2):488–492.

Marvin JS, Borghuis BG, Tian L, Cichon J, Harnett MT, Akerboom J, Gordus A, Renninger SL, Chen TW, Bargmann CI, Orger MB, Schreiter ER, Demb JB, Gan WB, Hires SA, Looger LL. An optimized fluorescent probe for visualizing glutamate neurotransmission. Nat Methods. 2013 Feb; 10(2):162–170.

Marvin JS, Scholl B, Wilson DE, Podgorski K, Kazemipour A, Müller JA, Schoch S, Quiroz FJU, Rebola N, Bao H, Little JP, Tkachuk AN, Cai E, Hantman AW, Wang SSH, DePiero VJ, Borghuis BG, Chapman ER, Dietrich D, DiGregorio DA, et al. Stability, affinity, and chromatic variants of the glutamate sensor iGluSnFR. Nat Methods. 2018 Nov; 15(11):936–939.

Owen MR, Doran E, Halestrap AP. Evidence that metformin exerts its anti-diabetic effects through inhibition of complex 1 of the mitochondrial respiratory chain. Biochem J. 2000 Jun; 348 Pt 3:607–614.

Park JO, Rubin SA, Xu YF, Amador-Noguez D, Fan J, Shlomi T, Rabinowitz JD. Metabolite concentrations, fluxes and free energies imply efficient enzyme usage. Nat Chem Biol. 2016 Jul; 12(7):482–489.

Pavlova NN, Hui S, Ghergurovich JM, Fan J, Intlekofer AM, White RM, Rabinowitz JD, Thompson CB, Zhang J. As Extracellular Glutamine Levels Decline, Asparagine Becomes an Essential Amino Acid. Cell Metab. 2018 Feb; 27(2):428–438.e5.

Qi L, Martin-Sandoval MS, Merchant S, Gu W, Eckhardt M, Mathews TP, Zhao Z, Agathocleous M, Morrison SJ. Aspartate availability limits hematopoietic stem cell function during hematopoietic regeneration. Cell Stem Cell. 2021 Aug; .

Studier FW. Protein production by auto-induction in high density shaking cultures. Protein Expr Purif. 2005 May; 41(1):207–234.

Sullivan LB, Gui DY, Hosios AM, Bush LN, Freinkman E, Vander Heiden MG. Supporting Aspartate Biosynthesis Is an Essential Function of Respiration in Proliferating Cells. Cell. 2015 Jul; 162(3):552–563.

Sullivan LB, Luengo A, Danai LV, Bush LN, Diehl FF, Hosios AM, Lau AN, Elmiligy S, Malstrom S, Lewis CA, Vander Heiden MG. Aspartate is an endogenous metabolic limitation for tumour growth. Nat Cell Biol. 2018 Jul; 20(7):782–788.

Tournaire G, Loopmans S, Stegen S, Rinaldi G, Eelen G, Torrekens S, Moermans K, Carmeliet P, Ghesquière B, Thienpont B, Fendt SM, van Gastel N, Carmeliet G. Skeletal progenitors preserve proliferation and self-renewal upon inhibition of mitochondrial respiration by rerouting the TCA cycle. Cell Rep. 2022 Jul; 40(4):111105.

Wheaton WW, Weinberg SE, Hamanaka RB, Soberanes S, Sullivan LB, Anso E, Glasauer A, Dufour E, Mutlu GM, Budigner GS, Chandel NS. Metformin inhibits mitochondrial complex I of cancer cells to reduce tumorigenesis. Elife. 2014 May; 3:e02242.

Zhang J, Fan J, Venneti S, Cross JR, Takagi T, Bhinder B, Djaballah H, Kanai M, Cheng EH, Judkins AR, Pawel B, Baggs J, Cherry S, Rabinowitz JD, Thompson CB. Asparagine plays a critical role in regulating cellular adaptation to glutamine depletion. Mol Cell. 2014 Oct; 56(2):205–218.

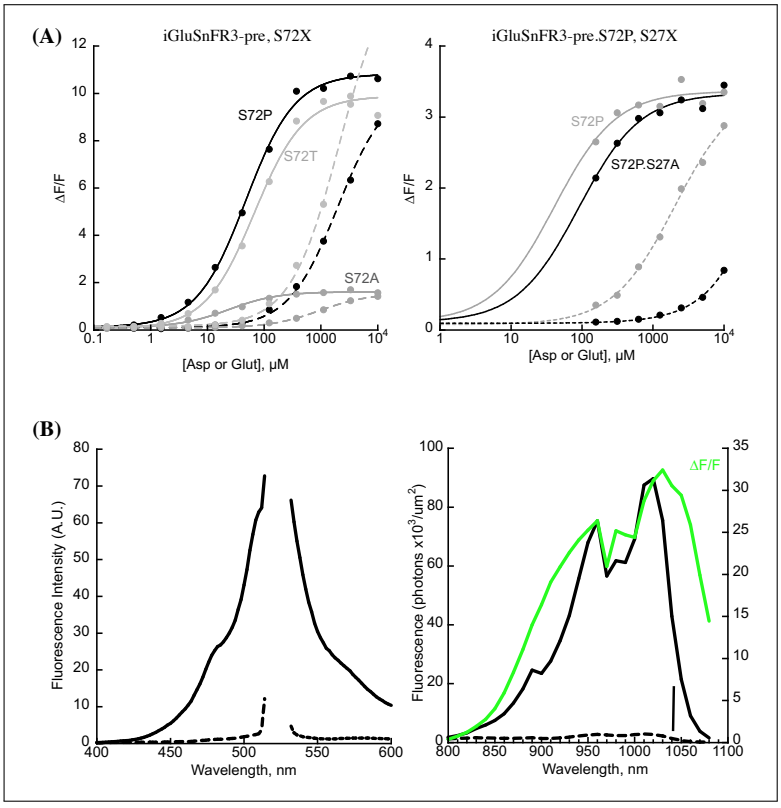

549

Figure 1—figure supplement 1. (A) Switching specificity of the iGluSnFR3 precursor from glutamate to aspartate using S72X library (left) and S72P, S27X library (right). Titrations with aspartate (solid lines) and glutamate (dashed lines) in bacterial lysate. (B) Excitation and emission spectra of jAspSnFR3-mRuby3. Left, 1-photon spectra. Excitation wavelength was varied from 400 nm to 520 nm (7.5 nm bandpass) while observing emission at 535 nm (10 nm bandpass). Emission wavelength was varied from 535 nm to 600 nm (10 nm bandpass) while exciting at 510 nm (7.5 nm bandpass). Fluorescence was measured both in the absence (dashed lines) and presence of 10 mM aspartate (solid lines). Right, 2-photon cross-sections, also ± 10 mM aspartate, with an overlay of calculated F/F (green). Vertical bar indicates 1040 nm.

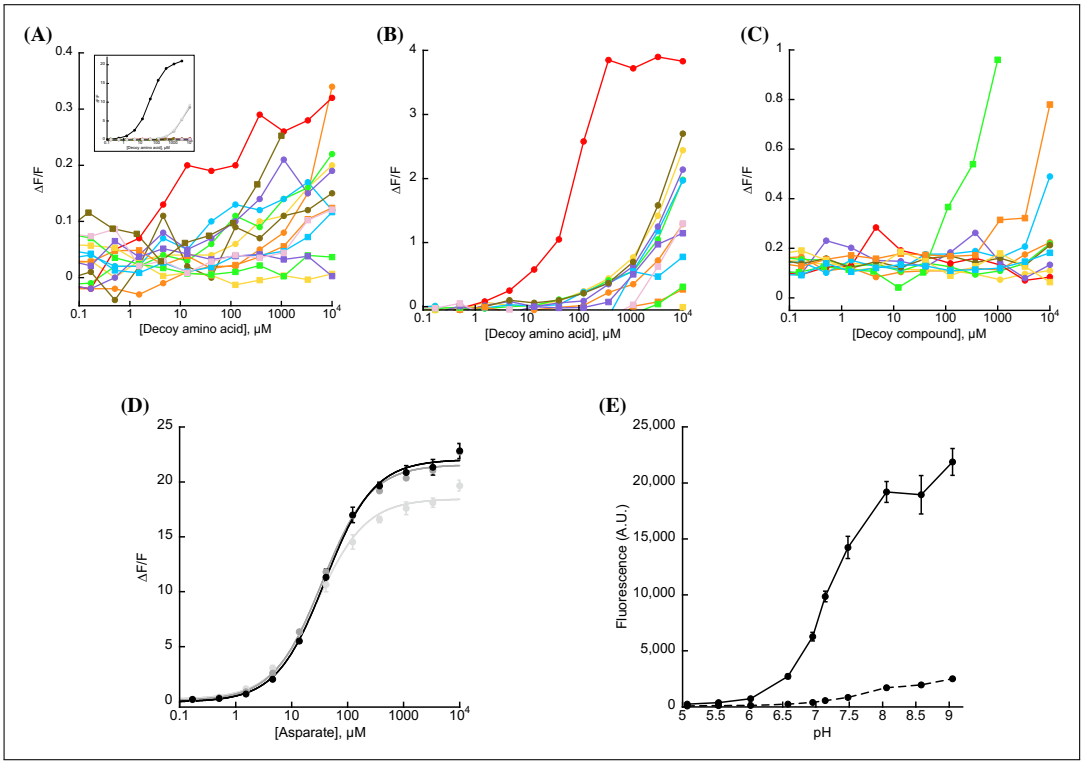

Figure 1—figure supplement 2. (A) jAspSnFR3-mRuby3 does not appreciably change its green fluorescence in response to other amino acids (alanine, phenylalanine, glycine, histidine (red line), isoleucine, leucine, methionine, proline, glutamine, arginine, serine, threonine, valine, or tryptophan). Insert with aspartate in black and glutamate/asparagine in grey for comparison. Ex. 485 nm (20 nm bandpass), Em. 535 nm (20 nm bandpass), 0.2 μM purified protein in PBS. (B) jAspSnFR3-mRuby3 shows increased red fluorescence at millimolar concentrations of all amino acids, with apparent responses to histidine at 100 μM (red trace). Ex. 587 nm (20 nm bandpass), Em. 662 nm (20 nm bandpass). (C) jAspSnFR3-mRuby3 does not respond to other decoys: citrate, lactate, pyruvate, malate, alpha-ketoglutarate, cis-aconitate, succinate, fumarate, or oxaloacetate (orange squares); nor to relevant pharmacological treatments: rotenone (green squares) or metformin. The small increase in fluorescence from rotenone is likely due to the scattering of a visibly turbid solution; rotenone has very low solubility in water. Ex. 485 nm (20 nm bandpass), Em. 535 nm (20 nm bandpass). (D) jAspSnFR3-mRuby3 is not adversely affected by temperature. Fluorescence as a function of aspartate titration at 23°C (light grey), 30°C (medium grey), and 37°C (black). Error bars are standard deviation of three technical replicates. (E) pH sensitivity of jAspSnFR3-mRuby3 (green component). Ex 485 nm (5 nm bp), Em 515 nm (10 nm bp). Error bars are standard deviation of 5 technical replicates. Solid line is with 3 mM aspartate, dashed line is without aspartate.

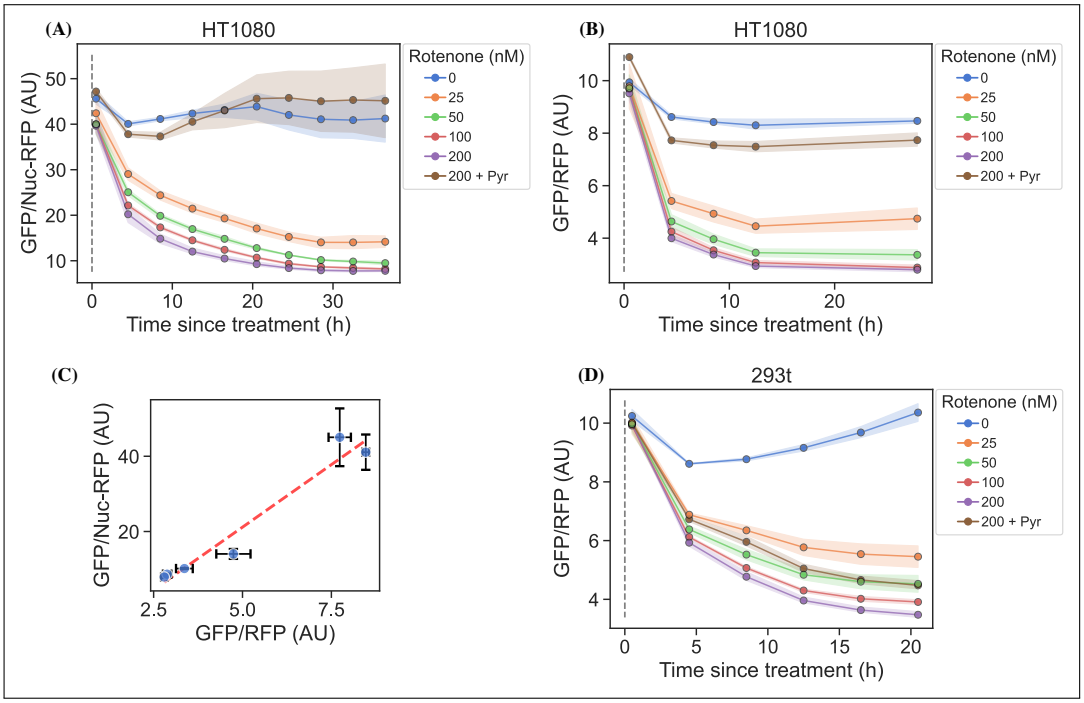

Figure 2—figure supplement 1. jAspSnFR3 temporal response after rotenone treatment. RFP normalized jAspSnFR3 signal change over time following rotenone treatment of live cells. Related to **Figure 2**, panel B; however, these experiments are not normalized to a pre-treatment scan. Grey dashed lines indicate the time of treatment and the first scan occurs 30 min after this. (A) HT1080 cells using nuclear RFP to normalize the jAspSnFR3 signal. (B) HT1080 cells using an RFP fused to jAspSnFR3 (jAspSnFR3-mRuby3) for normalization. (C) Comparison between the steady-state signal of (A) and (B) with a linear regression shown as a red dashed line to show that nuclear RFP and RFP fusion normalizations are equivalent. (D) HEK293t cells using an RFP fused to jAspSnFR3 for normalization. For plots (A), (B) and (D) markers indicate the average using available well replicates and are superimposed on a bootstrapped 95% confidence interval colored using the same color code as the markers. For plot (C) markers indicate the average using available well replicates and errorbars are drawn as +/- the standard deviation of the replicates. AU, arbitrary unit.

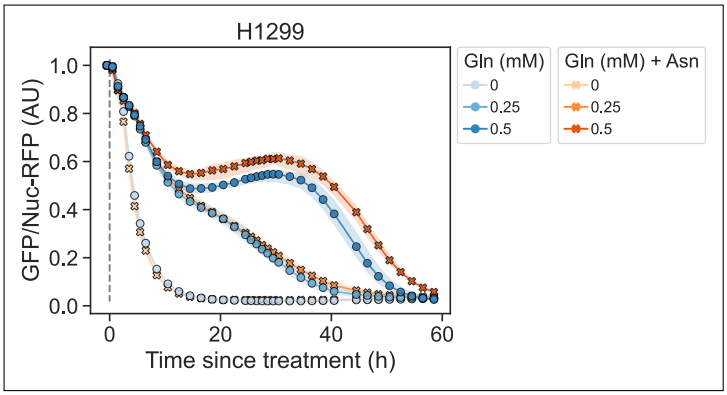

Figure 2—figure supplement 2. Aspartate depletes when glutamine is limiting. RFP normalized jAspSnFR3 signal change over time following glutamine depletion in H1299 cells. Identical to **Figure 2**, panel F but with fewer glutamine concentrations and more well replicates. AU, arbitrary unit.

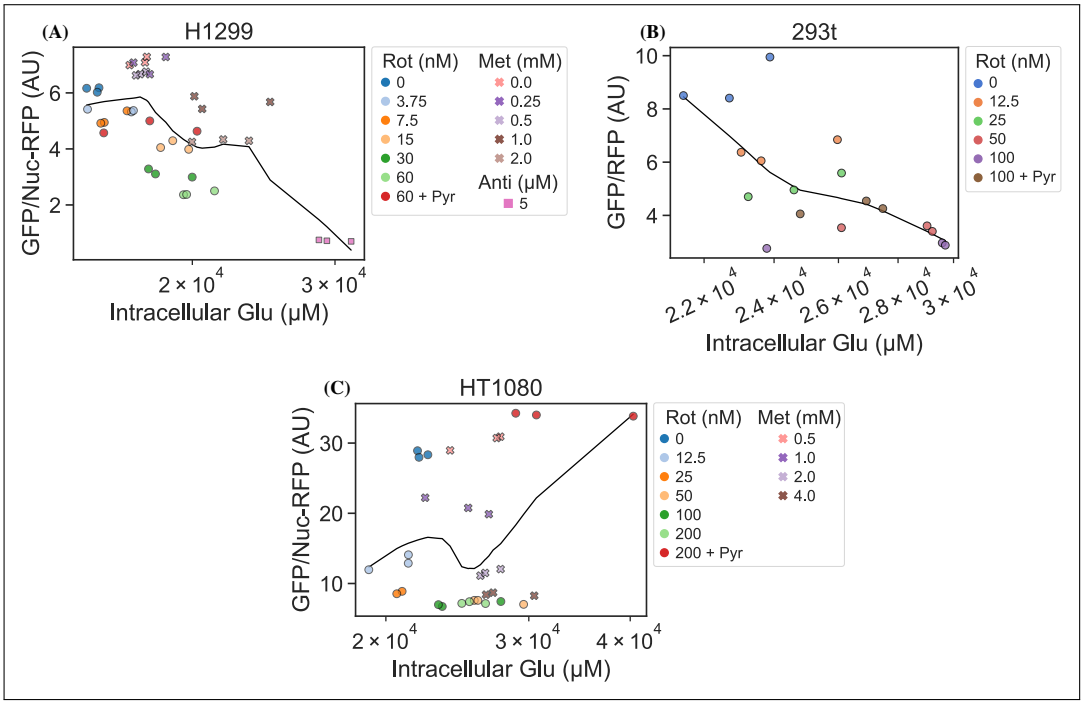

Figure 3—figure supplement 1. RFP normalized jAspSnFR3 signal, following various perturbations to live cells, is not correlated with the LCMS measured intracellular glutamate concentration. Datapoints are fitted to a local linear regression, shown by the black line, otherwise, these plots are identical to those in **Figure 3**. AU, arbitrary unit.